



Stability of Metal Matrix Composite Pads During High-Speed Braking

Tao Peng¹ · Qingzhi Yan¹ · Xiaolu Zhang¹

Received: 15 January 2018 / Accepted: 26 March 2018 / Published online: 4 April 2018
© Springer Science+Business Media, LLC, part of Springer Nature 2018

Abstract

Metal matrix composites are now commonly used as braking pads for the train running over 250 km/h by virtue of a number of desirable properties. To develop a fundamental understanding of the stability of metallic composites at high-speed braking, four typical composite materials, with different Cu and Fe contents, were subjected to a series of high-speed emergency braking at a simulative running speed of 380 km/h and a braking inertia of 27 kg/m^{-2} and a normal pressure of 1.27 MPa in this paper. The results showed that the sample with higher Cu content displayed a fade COF and deteriorated wear, but the one with higher Fe content could maintain a stable COF and low wear rate. The tribological behaviour is associated with the relative rate of generation and consumption of the tribo-oxide film. For the sample with higher Cu content, the generation rate of tribo-oxide film was less than the consumption rate, and the COF fading and wear deterioration with the increasing braking times were attributed to the reduction in resistance to deform or to shear the asperities, which was thought to be caused by the degradation of near-surface layer due to the removal of protective tribo-oxide film. In contrast, for the sample with higher Fe content, the generation rate was approximately equal to the consumption rate, and a well-established tribo-oxide film on the surface was responsible for the stable friction level and low wear rates.

Keywords Metal matrix composite pads · High-speed braking · Tribological behaviour · Stability

1 Introduction

Brake pad is a key component for high-speed train. To guarantee a safe, steady and durable brake system, pad materials generally should maintain a stable and reliable coefficient of friction (COF), irrespective of braking conditions, ambient temperatures and humidity [1, 2]. Cu-based metallic composites are now commonly used as brake pads for the train running over 250 km/h by virtue of many desirable properties, such as relatively high COF, high toughness, good thermal conductivity and moderate dent resistance [3–5]. Currently, high-speed train in China has already been running above 300 km/h; however, little research has been focused on the braking stability of these materials when subjected to high-speed braking, especially when speed is higher than 300 km/h [3, 5–7]. In general, it is desirable for the pad manufacturer to find a balance between the braking efficiency and braking stability.

High temperature induced by high-speed braking is often responsible for the irreversible transitions of material properties, such as softening, thermal elastic instability, degradation and thermal fatigue cracks, which can further result in the instability or fading of the pad materials [8–10]. Zhu et al. [11] found an unexpected fall in the friction coefficient for the brake shoe subjected to repetitious emergency braking and called it as “frictional catastrophe”. They believed that the phase transition from solid to liquid in the near-surface layer as a result of accumulated friction heat triggered this abnormal phenomenon. Verma et al. [12] demonstrated that the undesired wear deterioration of brake material is related to the removal of friction film, which is associated with the thermal decomposition of phenolic resins induced by high temperature. In our previous work, we also found a fading phenomenon associated with the broken of contact plateaus and local melting of some low melting-point phases at 380 km/h [13]. Therefore, it is deducible that a stable tribological behaviour relies on a stable microstructure of the contact surface.

It is generally acknowledged that the tribological behaviour is determined by the structural, chemical and mechanical characteristics of the friction film [14–16]. As Jacko et al.

✉ Qingzhi Yan
qzyan@ustb.edu.cn

¹ University of Science and Technology Beijing, Beijing, China

described in [17], “When stable friction films, commonly called friction layers, are readily formed for a given friction couple, a stable friction level and low wear rates can be maintained at various temperatures, as long as the friction film is not destroyed”. In our recent work [18], two commonly used ingredients, Cu and Fe, were found to play distinct roles in the friction film of the composite pad. The latter seems to more likely to form a steady tribo-oxide film on the friction surface. Therefore, it is interesting to find out the relationship between the braking stability and the Cu/Fe ratio of the composite pads.

Considering the importance as well as a current lack of understanding of the braking stability of metal matrix composites under extreme conditions, in this paper, four typical pad samples, with different Cu and Fe contents, were applied to a series of high-speed braking by a sub-scale braking tester. The tests simulated an extreme case, in which the train underwent a repetitious emergency braking with a running speed of 380 km/h. The generation or consumption of tribo-oxide film as well as the change in wear debris was correlated to the tribological stability of pad in the context.

2 Experiments

2.1 Fabrication of the Composites

The ingredients, Cu (4–7 μm , 99.5% pure), Fe (10–18 μm , 99% pure), graphite (250–500 μm , 97% pure), ferrochrome alloy (Cr–Fe) (120–250 μm , 98% pure), MoS_2 (18–48 μm , 99% pure), SiO_2 (58–120 μm , 99% pure), binder, etc., were used to keep as consistent as possible with the ingredients used in commercial pad. Four samples, S1, S2, S3 and S4, were prepared based on keeping parent composition of some ingredients (32 wt%) constant and varying two ingredients, i.e. Cu and Fe, in a complementary manner to ensure the ratio of Cu/Fe decrease proportionately (Table 1). More details of the preparation methods can be found in our previous work [18]. Figure 1 shows the backscattered electron (BSE) images of the sintered samples, in which some of the components are indicated based on the energy-dispersive X-ray spectrometry (EDS) identification. Note that the light-grey regions in Fig. 1e represent Cu matrix and the grey regions are Fe matrix. Besides, some components, like graphite, Cr–Fe particles and SiO_2 , preserved the original

powder appearances. The physical and mechanical properties of the samples, such as porosity, density, Brinell hardness and shear strength, can also be found in [18]. The nominal contact surface of the brake pad was 1787 mm^2 . The rotor disc was 450 mm in diameter and 35 mm in thickness and made of forged steel (30CrSiMoVA) with 30–35 HRC hardness, which is one of the conventional materials in current high-speed-train in China.

2.2 Braking Tests

The braking tests were carried out on a sub-scale testing apparatus (TM-I, Xi’an Shun Tong Technical Research Institute, China. Figure 2) at an ambient temperature of 15 $^\circ\text{C}$ and a relative humidity of 40% in the pad-on-disc configuration, and more details about the tester can be found in [13]. To investigate the stability of pad samples subjected to extreme conditions, a series of twelve repetitious high-speed emergency braking tests was performed. The applied initial rotation speed was 3980 rpm (65 m/s in linear velocity), corresponding to the initial braking speed (IBS) of the train up to 380 km/h. Based on a scale-conversion rule [19], the braking inertia and the normal pressure were set as 27 kg/m^{-2} and 1.27 MPa, respectively, to simulate 16 tons of mass to be stopped per disc in the real train under the emergency braking.

During each test, the braking disc was equipped as a rotator of the test machine and driven by an AC motor to a certain rotating speed, i.e. the IBS. Then, two fixed braking pads, equipped as the stators of the machine, were pressed to the braking disc simultaneously, resulting in a mean friction radius of 155 mm and a nominal contact area of 1787 mm^2 . When the rotator reached the given speed, it was cut off from the motor and slowed down consequently due to the drag of pad friction. Then, the mean COF, μ_t , was automatically calculated by the computer system based on Eq. (1):

$$\mu_t = \frac{\int_0^{t_s} \mu dt}{t_s} \quad (1)$$

where μ is the transient COF and t_s is the stopping time. The stability coefficient, α_s , which is used to describe the fading behaviour of the pad subjected to twelve repetitious high-speed braking tests, was defined as Eq. (2):

Table 1 Details of the formulated composites (wt%)

Sample	Cu	Fe	Cr–Fe	Graphite	MoS_2	SiO_2	Others	Ratio of Cu/Fe
S1	60	8	8.0	10	2.5	5.0	6.5	7.5
S2	48	20						2.4
S3	30	38						0.79
S4	14	54						0.26

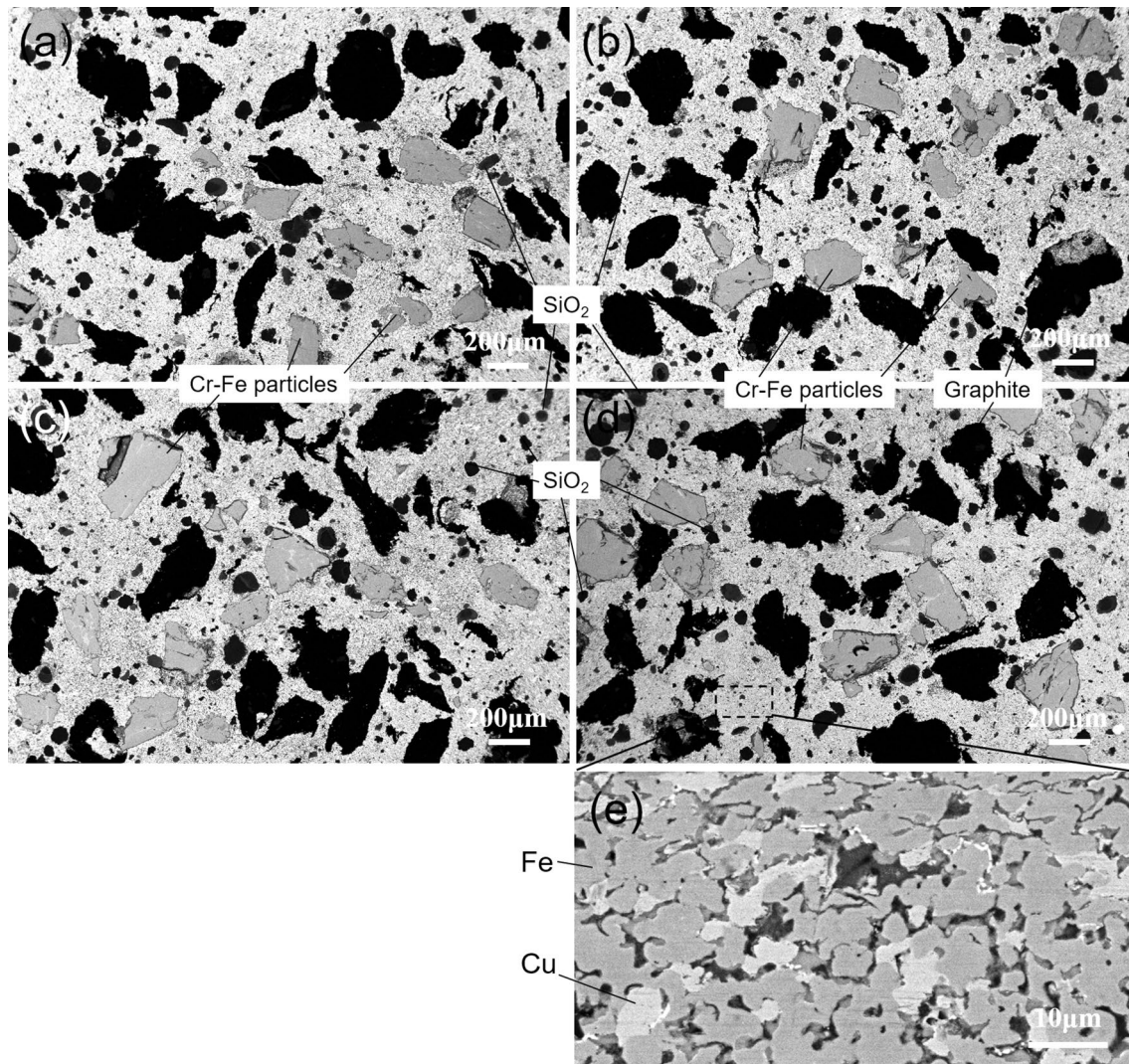


Fig. 1 Backscattered electron images (BSE) of the sintered pads, in which some of the components are indicated. **a** S1, **b** S2, **c** S3, **d** S4, **e** high-magnification SEM image of the frame in **d**

$$\alpha_s = 1 - \frac{\mu_{\max} - \mu_{\min}}{\bar{\mu}} \times 100\% \quad (2)$$

where $\bar{\mu}$ is the average of the mean COFs among the twelve tests and μ_{\max} and μ_{\min} are the maximum one and the minimum one, respectively. The wear rate, W_r , of the pad samples was determined by measuring their weights before and after testing in an analytical balance (D&T ES5000, with an accuracy of 0.01 g). Data were then converted into wear volumes, V , using the measured density of the pad samples. The W_r was calculated by normalizing the wear volumes by the dissipated energy, E_s , using Eq. (3):

$$W_r = V/E_s \quad (3)$$

Similarly, the stability coefficient of wear rate could be obtained by replacing μ by W_r based on Eq. (2).

The disc wear was determined by measuring the thickness of wear trace before and after each completely 12 times braking with a micrometre calliper (0.01 mm in accuracy). To rule out the influence on the result from thermal expansion, we performed the measurements after the disc cooled to room temperature. The wear losses of the disc against different samples after each completely test were less than 0.01 mm, which were negligible relative to the pad wear.

The subsurface temperatures of the pad and the disc were measured by two thermocouples located 2 mm beneath the contact surface within the pad and the disc, respectively. It should be noted that the measured disc temperatures were less than 600 °C in all period of time with regard to all the samples, which were lower than the phase-transition temperature of the steel disc. Before each test, the wear trace of the disc surface was abraded by SiC abrasive papers of

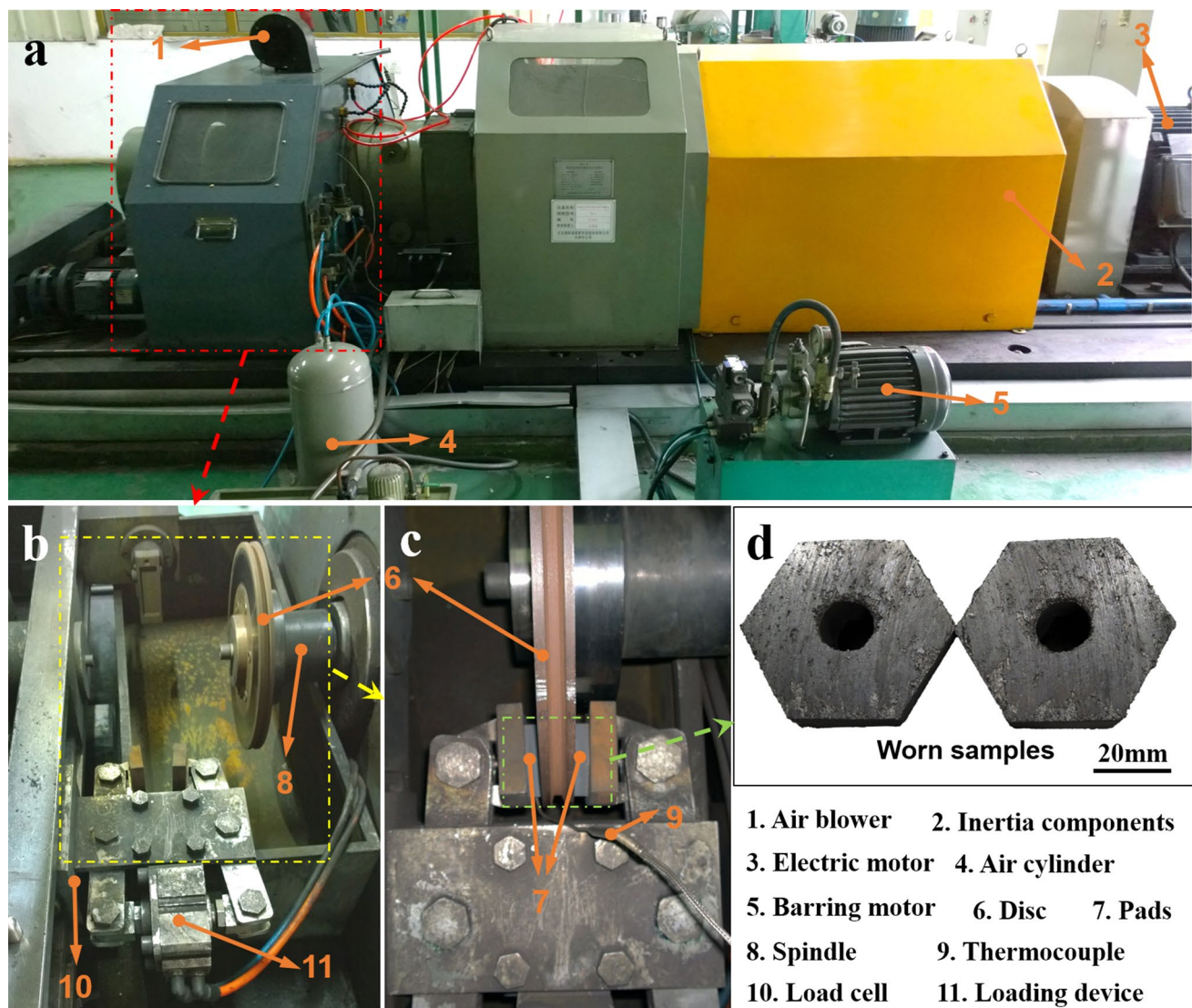


Fig. 2 Schematic diagram of the sub-scale brake testing apparatus. **a** External diagram; **b** inside diagram; **c** pad-on-disc configuration; **d** friction pads

various grit sizes to eliminate the protrusions and residual transfer layers from previous tests. The roughness (R_a) of disc surface was adjusted to 1.5–2.0 μm as measured with a portable profilometer (Beijing Time-Top Technology Co., SF200, China) after the abrasion process. And then, we measured the hardness of the disc (9 times test) in different positions of the wear trace using a portable Leeb hardness tester (Beijing Time-Top Technology Co., HL-200, China). All the values were in the range of 41–45 HRC, which were slightly higher than that of the original disc (30–35 HRC), owing to the strain hardening during braking. Next, we conducted seven times run-in brakes with an IBS of 25 m/s and a normal pressure of 1.27 MPa to ensure a favourable contacting surface between the pad and the disc. For ensuring the same initial conditions for each stop-braking test,

it was not until the surface temperature of pad dropped to 50 $^{\circ}\text{C}$ that the next test could be conducted. To ensuring the reliability of the experiment's data, each completely twelve repetitious braking tests were repeated three times and the mean values (mean COF and mean wear rate) of three are reported for each data point.

2.3 Characterization Techniques

Physical properties and mechanical properties of the braking pad, including density, porosity, hardness, shear strength and compressive strength, were tested according to China Railways Production Certification Center standards (CRCC, TB/T 3470-2016). On the other hand, a pull-up peeling test involving epoxy bonding a 6-mm-diameter stud to the

friction surface was conducted on the different pads to reveal the strength of the near-surface layer. More details of this method can be found in [18].

Scanning electron microscopy (SEM, ZEISS, LEO1450, Germany) attached with energy-dispersive X-ray spectrometry (EDS, OXFORD, 51-XXM, UK) was applied to examine the surface and vertical section morphologies of the worn pads as well as to analyse the constituents in the friction surface. Surface roughness (S_a) of the worn surfaces was quantified by laser confocal microscopy (LCM, OLYMPUS, OLS4100, Japan). For identifying the crystalline phases of wear debris, X-ray diffraction (XRD, Rigaku, SmartLab, Japan) measurements were carried out.

3 Results

3.1 Braking Behaviours of the Different Pad Samples

Figure 3 shows the evolution of the COFs with increasing braking times with respect to different pads. It is interesting to note that there exist two different trends of COF curves: the COFs of S1 and S2 firstly decreased (from 0.37 and 0.348 to 0.323 and 0.313, respectively) with increasing braking times, which demonstrated a fading phenomenon, and then reached a steady state after 7 times braking. In contrast, the COFs of S3 and S4 are about 0.31 and 0.28, respectively, which seem more stable than S1 and S2 throughout all the periods. The stability coefficients of S1, S2, S3 and

S4 were 86.4, 89.8, 92.7 and 93.6%, respectively, which suggests that the fading was alleviated with the increase in Fe content. On the other hand, the mean COFs decreased with the increase in Fe content, irrespective of the braking times. It should be noted that this result is not occasional because of the repeated experiments we made and the similar results obtained.

Figure 4 shows the evolution of wear rates with increasing braking times. The wear rate curves also display two different trends: the wear rates of S1 and S2 increased with the increasing times and reached a steady state finally. The wear rates of S3 and S4 almost remained constant at 0.17 and 0.16 cm^3/MJ , respectively. In addition, the wear rates also decreased with the increase in Fe content, and the wear rate of S1 was considerably larger than that of the other three.

Figure 5 shows the average maximum subsurface temperatures (T_{max}) of the different pads under repetitious braking tests. The T_{max} slightly decreased with the increase in Fe content of the pad, owing to the decrease in the dissipation of frictional power. Considering the measured T_{max} represented the bulk temperature 2 mm beneath the contact surface, the real temperature of contact sites must far above the value recorded.

3.2 Evolution of the Worn Surfaces

As presented above, the distinct behaviours of the COFs and wear rates with regard to different pads implied different tribological mechanisms. To explore the braking stability of the pads subjected to repetitious high-speed braking, we

Fig. 3 Evolution of the COFs with increasing braking times with respect to different pads. The inserted labels show the stability coefficient of the corresponding curve

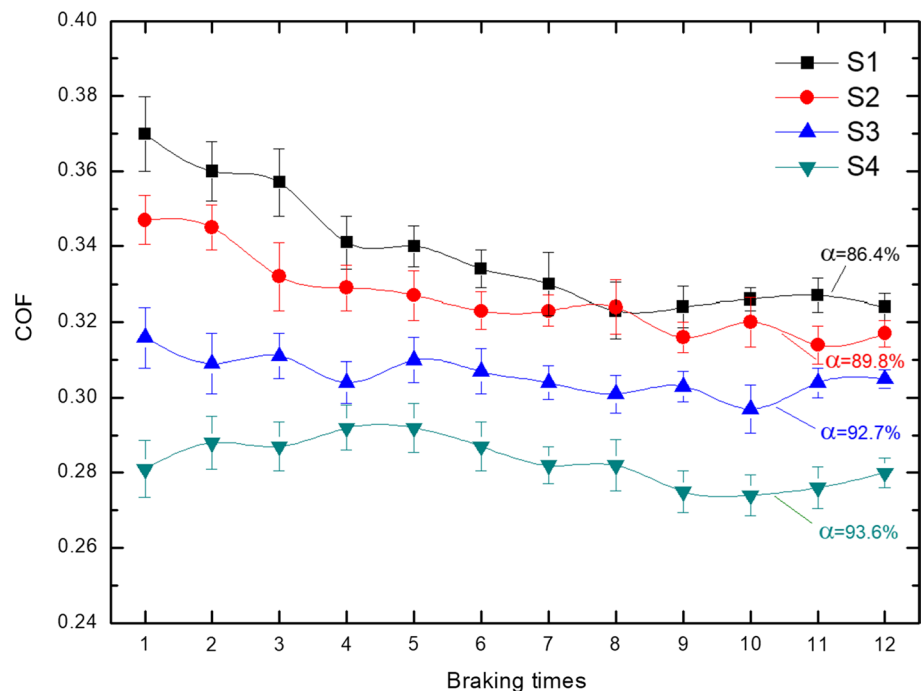


Fig. 4 Evolution of wear rates with increasing braking times with respect to different pads. The inserted labels show the stability coefficient of the corresponding curve

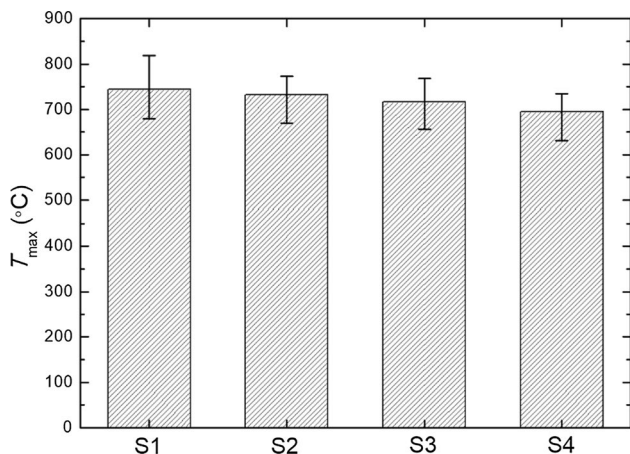
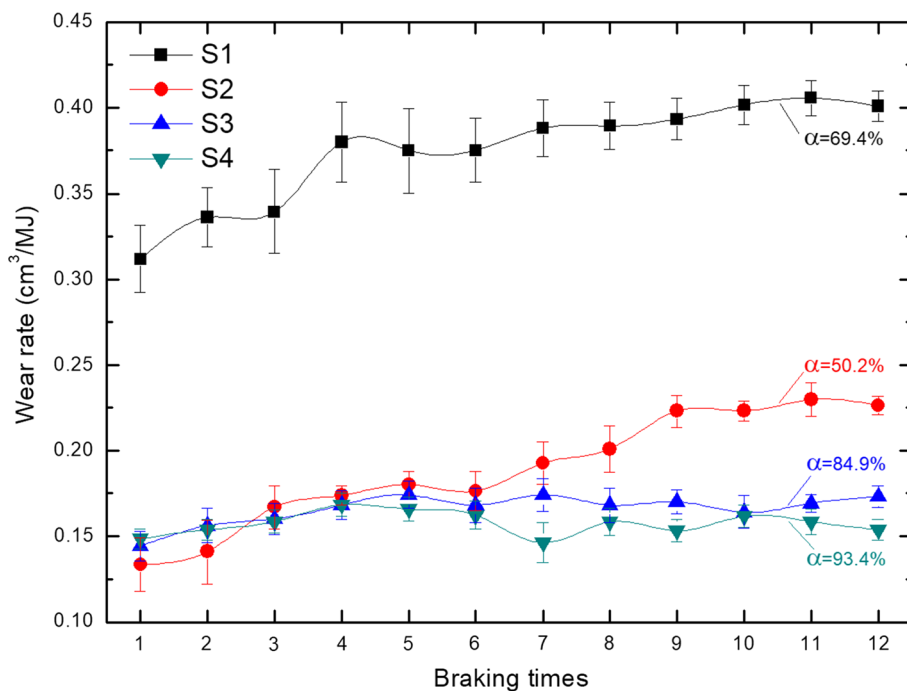


Fig. 5 Maximum subsurface temperatures (T_{max}) of the different pads

herewith selected the representative worn pads from different periods for further observation.

The microstructure evolutions of the friction surfaces of S1 and S4 with increasing braking times are totally different (Fig. 6). The friction surface of S1 showed typical delamination wear and was partly covered by the tribo-oxide film after 2 times braking based on the EDS identification (Fig. 7a). This friction surface was gradually destroyed, and the delamination became more and more remarkable with the increase in braking times (Fig. 6b, c). Just like what we found in [13], it is easy to find some exposed graphite particles in the fracture zones (Fig. 6b, c), indicating that the graphite/matrix interface might be a source of the

delamination fracture. However, it seems no change in the microstructures of the friction surface of S4 with increasing braking times (Fig. 6d–f). This friction surface was dominated by a quite smooth tribo-oxide film (Fig. 7b), in addition to containing a few exposed graphite particles and small peeling pits.

On the other hand, the representative vertical section views (parallel to the sliding direction) are shown in Fig. 8. Numerous defects, such as delamination cracks and fracture zones, suggest the friction surface of S1 was already destroyed after 2 times braking, although the surface was also covered by a certain scale of tribo-oxide film (Fig. 8a). With the braking times increased, the tribo-oxide film was absent from the surface and the fracture zones got thicker due to wear damage (Fig. 8b, c). Conversely, the surface of S4 was covered by a complete tribo-oxide film with the thickness of about 50 μm (Fig. 8d–f), irrespective of the braking times.

The microscopic morphologies of the friction surfaces observed by LCM at different periods are shown in Fig. 9. The fracture zones on the friction surface of S1 were continuously expanded and deepened with the increase in braking times, and the corresponding S_a increased from 12.7 to 20.4 μm (Fig. 9a–c). However, there were no obvious distinctions in the S_a between the three periods with respect to S4, with the value in the range from 6.8 to 8.2 μm (Fig. 9d–f). These results are in consistent with the microstructure evolutions observed by SEM (Figs. 6, 8).

Figure 10 shows the peeling strengths of the friction surfaces at different periods. This value can be used to

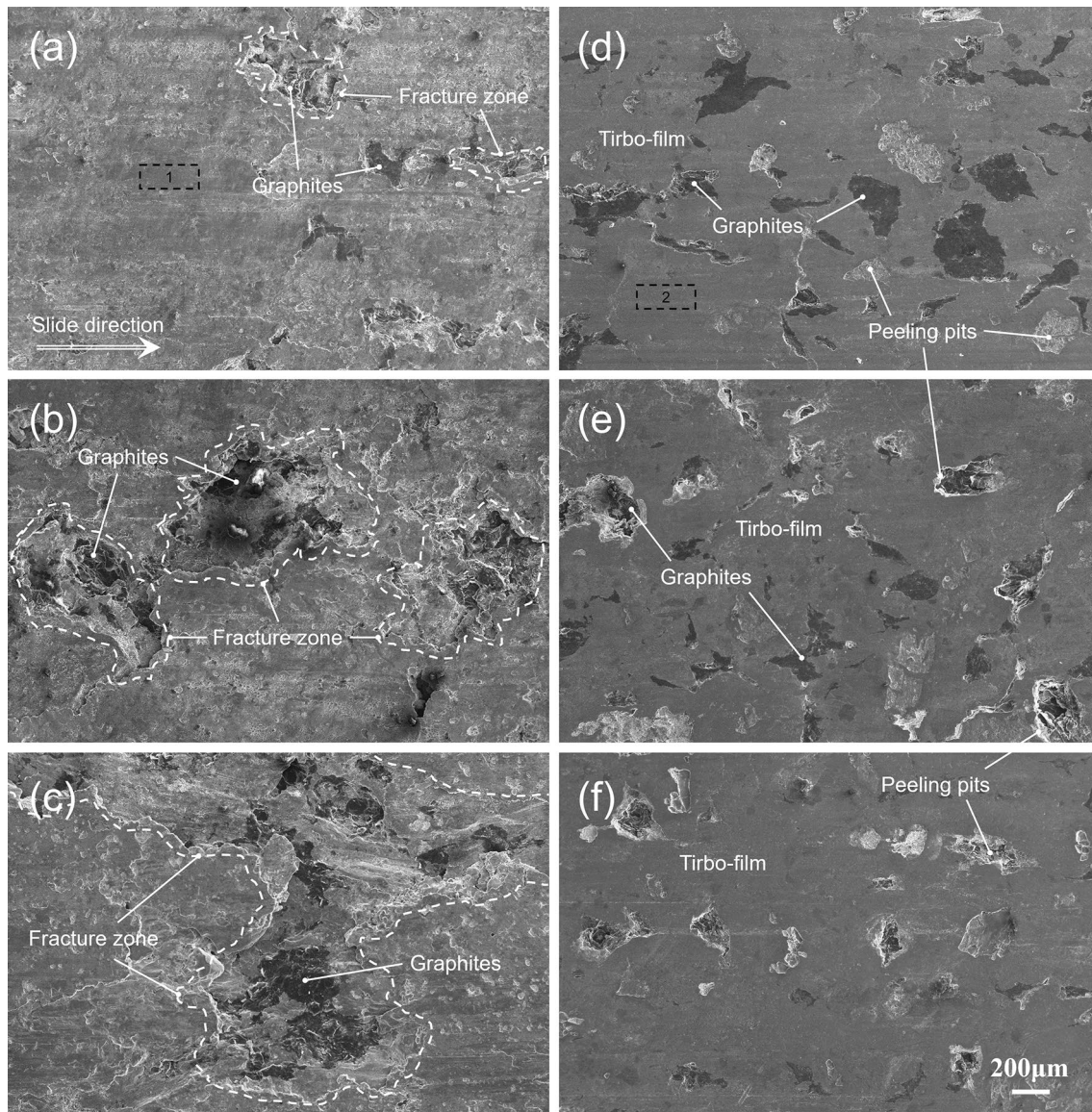


Fig. 6 Microstructure evolutions of the friction surfaces with increasing braking times. **a** S1, 2nd; **b** S1, 7th; **c** S1, 12th; **d** S4, 2nd; **e** S4, 7th; **f** S4, 12th. The bar scale is same for all the images

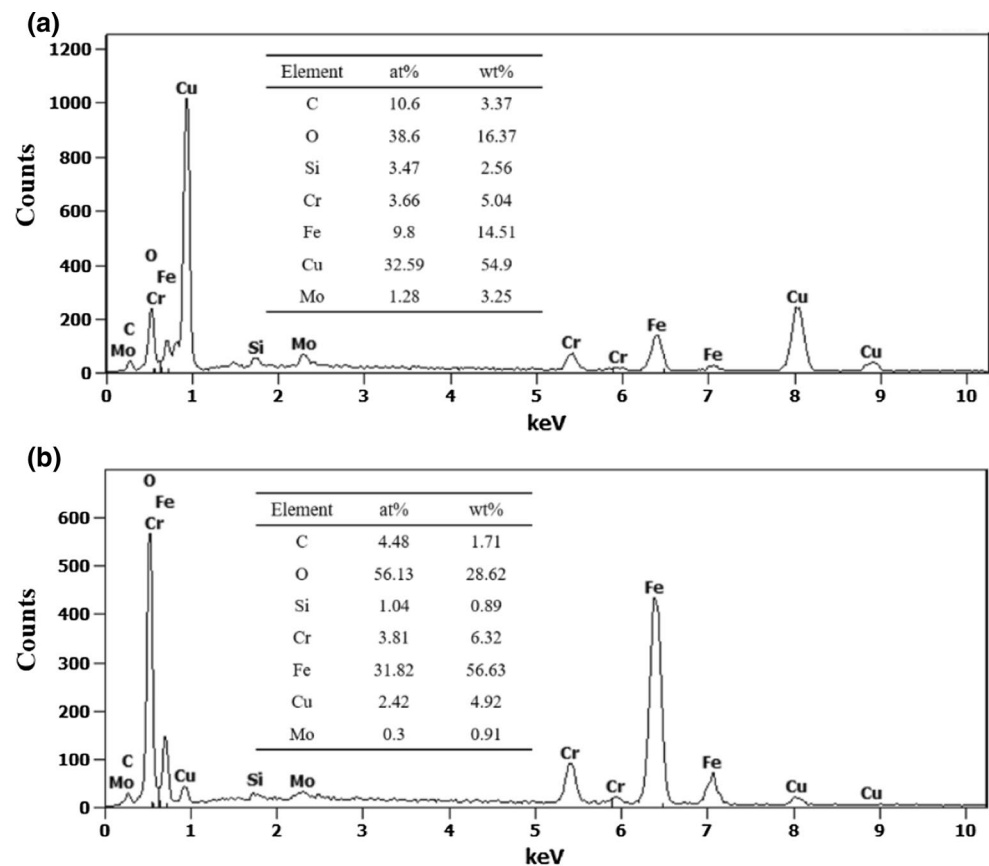
reflect the capability to resist destruction within the near-surface layer, as interpreted in [18]. Note that the peeling strength of S4 was much higher than that of S1 for all the periods, which may be attributed to a protective tribo-oxide film covered on the surface of S4. With the increase in braking times, the average peeling strength of S1 decreased from 1.62 to 0.71 MPa, while it was nearly constant for S4 with the value of about 3 MPa. It means that the capability to resist destruction within the near-surface was decreased with increasing braking times with respect to S1.

3.3 Analysis of Wear Debris

The microstructure and phase composition of the wear debris can reflect the wear mechanism and the physical and chemical changes in the process of braking. To further reveal the different tribological behaviours of the pads investigated, we herewith focused on the analysis of wear debris.

The microstructures of the wear debris are shown in Fig. 11. The different microstructures between the wear debris of S1 and S4 implied different wear modes under the braking condition. The wear debris of S1 mainly consisted

Fig. 7 EDS patterns exhibiting the chemical compositions of: **a** pane “1” in Fig. 6a; **b** pane “2” in Fig. 6d



of large fragments, like sheets and lumps, in which some graphite inclusions could be observed (Fig. 11a), indicating a deep fracture source and a severe delaminated wear mode. By contrast, the smaller fragments, like chips and granule, suggest that the mild delamination and oxidation were the predominant wear regimes with respect to S4. Such findings suggest that the near-surface layer of S1 was more vulnerable than that of S4, which was in accordance with the peeling strength behaviours of the friction surfaces (Fig. 10).

Figure 12a, b shows the compositional variation of the wear debris under different braking times with regard to S1 and S4, respectively. For S1 sample, the peak intensities of the original phases, like Cu and C, were significantly higher than that of the tribo-oxides, Cu_2O and Fe_3O_4 . And the phase composition of the wear debris was similar to that of the original material. Besides, the intensities of Cu_2O and Fe_3O_4 peaks decreased with the increase in braking times, while the intensities of Cu, C and SiO_2 peaks displayed opposite trends. Combined with the weak surface and severe delamination of S1, the variation of debris compositions may reveal that the tribo-oxidation barely had time to occur when the surface was worn, and the time used for tribo-oxidation became shorter with increasing braking times. In comparison with S1, Fe_3O_4 was the dominated phase throughout all the periods with regard to S4, while the peak of Fe was

unobservable. Meanwhile, it seems no change in the peak intensities of all the phases (Cu, Fe_3O_4 , $\text{Fe}_{0.95}\text{O}$ and C) at different periods. These mean that there was a significantly tribo-oxidation on the contact surface of S4 during braking, and the tribo-oxide film was stable, irrespective of the braking times.

4 Discussion

From the above-mentioned description, there were totally distinct tribological behaviours between the samples of Cu/Fe ratio > 1 and the samples of Cu/Fe ratio < 1, and the former displayed a fading phenomenon, while the latter showed a good stability. Besides, the higher the Fe content for the sample, generally, the lower the mean COF and wear rate for a certain braking time. Meanwhile, the samples display different variations in the aspects of tribofilm morphology, wear debris microstructure and composition, resulted from the tribo-oxidation, compaction and fracture on the rubbing surfaces. The tribofilms can separate the original two bodies (i.e. composite pads and steel disc) and are beneficial to the decrease and stabilization in friction, owing to a tendency to suppress metal-on-metal contact [17, 20–23], which commonly corresponds to the onset of adhesion and large

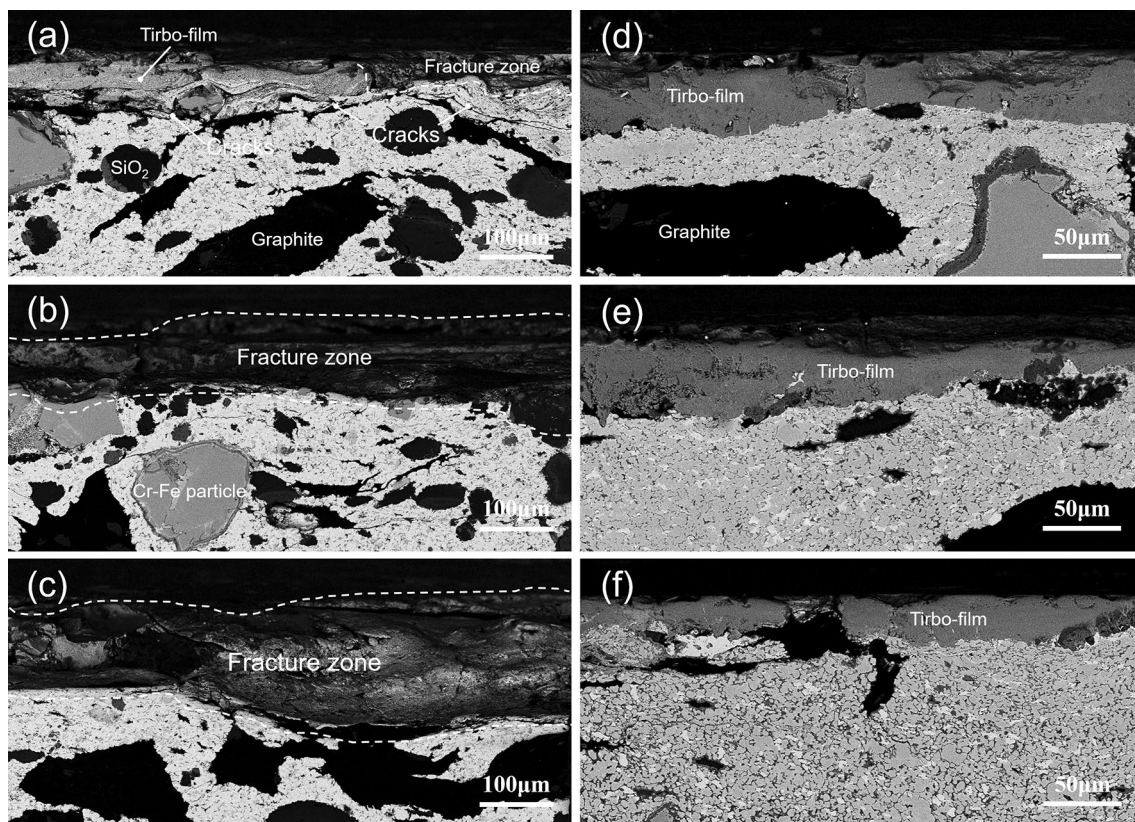


Fig. 8 Representative vertical sectional microstructures of the friction surfaces. **a** S1, 2nd; **b** S1, 7th; **c** S1, 12th; **d** S4, 2nd; **e** S4, 7th; **f** S4, 12th

volume of plastic deformation, which is considered to be the primary approach of energy dissipation during friction [24]. Such an effect had been visually presented in Österle et al.'s works [25, 26], in which the cases of oxide-on-oxide and metal-on-metal contacts were compared based on a movable cellular automata (MCA) method. What is more, at the high temperatures, the tribofilms, produced by the compaction and tribosintering of oxidized wear debris, were also found to play a protective role on the friction surface, which is associated with a transition from severe wear to mild wear [27–29]. Therefore, the tribological performance can be correlated with the relative rate of generation (ω_g) and consumption (ω_c) of the tribofilm, which is thought to be related to the oxidative thermodynamics and kinetics of metallic matrix, fragments bonding and interfacial adhesion.

It is known that iron is more easily oxidized than copper based on Ellingham diagram (Fig. 13) [30]. The tribo-oxide film thereby would be more easily to form on the friction surface with regard to the sample containing more Fe. On the other hand, the destruction of the tribo-oxide film can be correlated with the adhesion of tribo-oxides/substrate or the bonding strength of graphite/metals interfaces [31]. The thermal expansion coefficient ratio of Fe to FeO, Fe₃O₄ and Fe₂O₃ is 1.25, 1.46 and 1.39 [32], respectively, which is far below that of Cu to Cu₂O (4.3) [33]. Therefore, the

tribo-oxide film containing more iron oxides may adhere tighter to the substrate due to less thermal stress (tensile stress) induced by friction heat during braking. In addition, since the wettability between Fe and graphite is better than that between Cu and graphite (neither mutual dissolution, nor to form a stable carbide), the bonding strength of Fe/graphite interface may be higher than that of Cu/graphite interface. The tribo-oxide film would be more hardly to destroy on the friction surface with regard to the sample containing more Fe. Therefore, the sample with higher Fe content showed lower mean COF and wear rate could be attributed to the better established tribo-oxide film on the surface.

In the samples of Cu/Fe ratio > 1, because of the inferior oxidative thermodynamics of Cu [30], higher thermal expansion coefficient ratio of Cu to Cu₂O [33], and poorer bonding strength of Cu/graphite interface, as mentioned above, the tribo-oxide film was hard to form but easy to destroy on the surface, i.e. $\omega_g < \omega_c$. Thus, the tribo-oxide film was continuously removed from the surface (Figs. 6a–c, 8a–c). Consequently, with the increase in braking times, the near-surface layer of S1 was damaged gradually and the defects were increased within this region (Figs. 6a–c, 8a–c), leading to the decrease in the peeling strength of the friction surface (Fig. 10). Meanwhile, due to the lack of protective

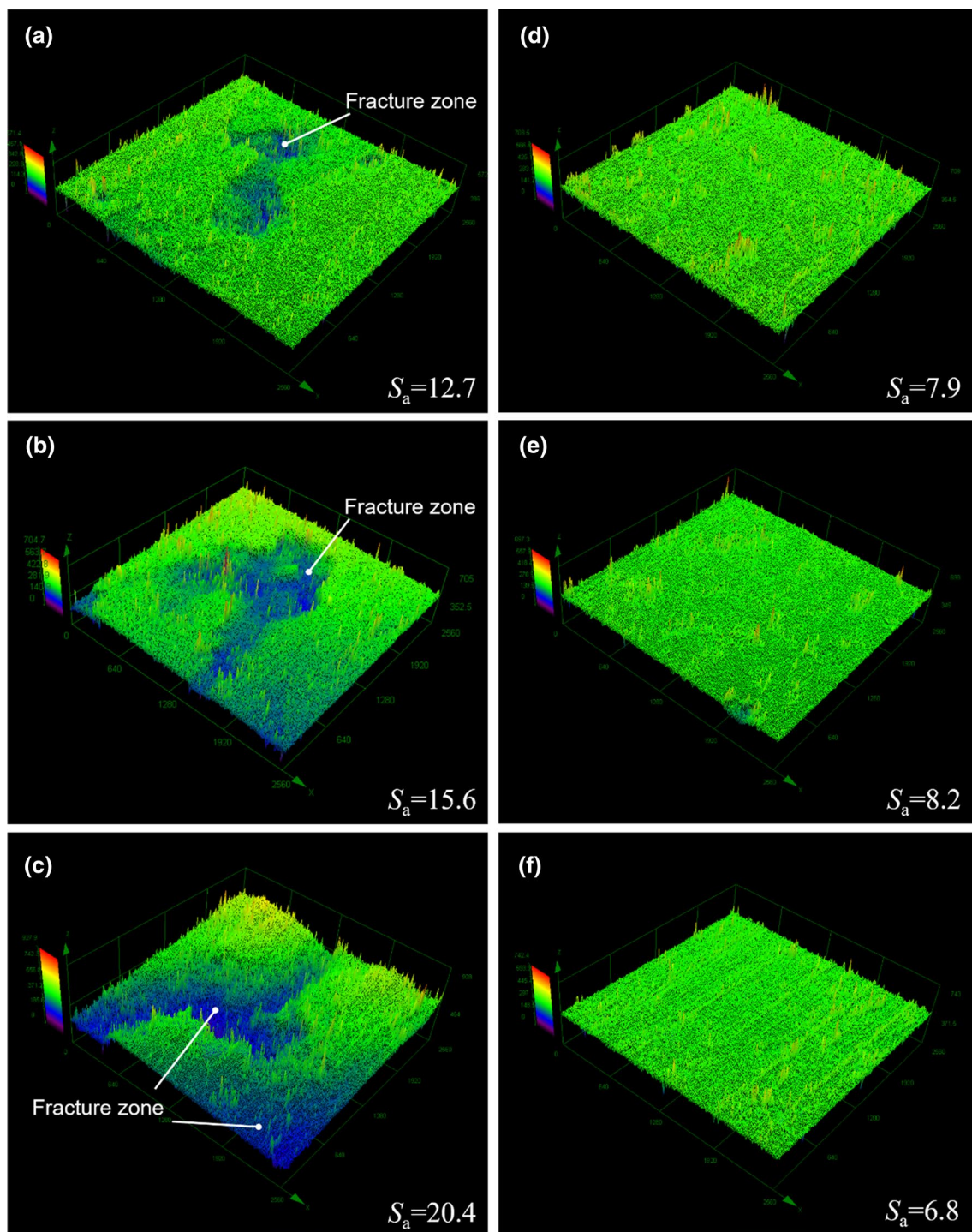


Fig. 9 Typical microscopic morphologies of the friction surfaces based on LCM, with the corresponding surface roughness (S_a) in the bottom right corner. **a** S1, 2nd; **b** S1, 7th; **c** S1, 12th; **d** S4, 2nd; **e** S4, 7th; **f** S4, 12th

tribo-oxide film, the flawed matrix was directly subjected to wear damage to form sheet and lump debris, in which most of the original compositions were maintained and only slight tribo-oxides were generated; and as braking times increased, the percentage of the original compositions and tribo-oxides

in the debris increased and reduced, respectively, because the composite barely had time to oxidize when the surface was worn (Fig. 12a). It is known that the frictional force is generated as a consequence of asperities deformation and shear within the adhesion junctions [34], and the generated

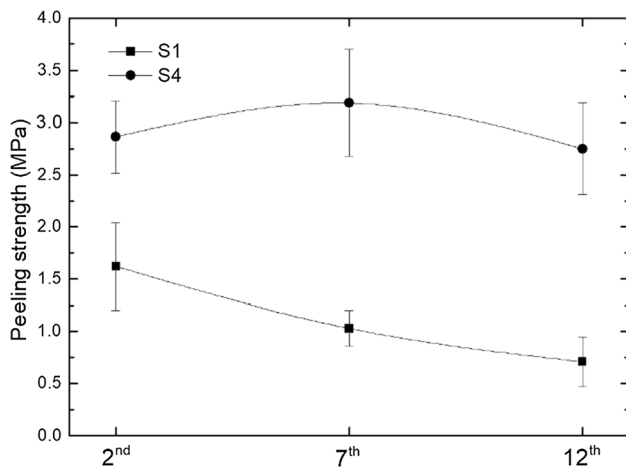


Fig. 10 Peeling strengths (MPa) of the friction surfaces as a function of braking times

stress is supported by the near-surface layer. If there are already numerous defects within this region, the asperities would become weak due to the lack of enough load-bearing capacity, requiring a correspondingly small force to deform or to shear the contact areas. In this case, the energy is easily dissipated by crack propagation and delamination (producing new interface), which may be responsible for the COF fading and wear deterioration with respect to the samples of Cu/Fe ratio > 1 .

By contrast, in the samples of Cu/Fe ratio < 1 , higher Fe content accelerated the formation of the tribo-oxide film and in turn inhibited the destruction of the tribo-oxide film on the surface, contributing to a comparable generation

rate and consumption rate with regard to the tribo-oxide film, i.e. $\omega_g = \omega_c$. As a consequence, the tribo-oxide film was well established on their surfaces. The microscopic morphologies (Figs. 6d–f, 8d–f, 9d–f) and strengths (Fig. 10) of the friction surfaces as well as the wear debris compositions (Fig. 12b) could remain stable, irrespective of the braking times, and a stable friction level and low wear rates were maintained at all the periods.

5 Conclusions

1. The sample with the Cu/Fe ratio > 1 and the one with the ratio < 1 demonstrated totally distinct tribological behaviours, the former displayed a fade COF and deteriorated wear, while the latter maintained a stable friction level and low wear rates at all the periods.
2. There exists a strong correlation between the tribological behaviour and the relative rate of generation (ω_g) and consumption (ω_c) of the tribo-oxide film.
3. In the cases of Cu/Fe ratio > 1 , tribo-oxide film was hard to form but easy to destroy on the surface. The COF fading and wear deterioration increased with the increase in braking times because of the reduction in resistance to deform or to shear the contact areas, which was thought to be caused by the degradation of near-surface layer due to the removal of protective tribo-oxide film.
4. In the cases of Cu/Fe ratio < 1 , higher Fe content contributed to form a stable tribo-oxide film on the surface, leading to a stable friction level and low wear rates.

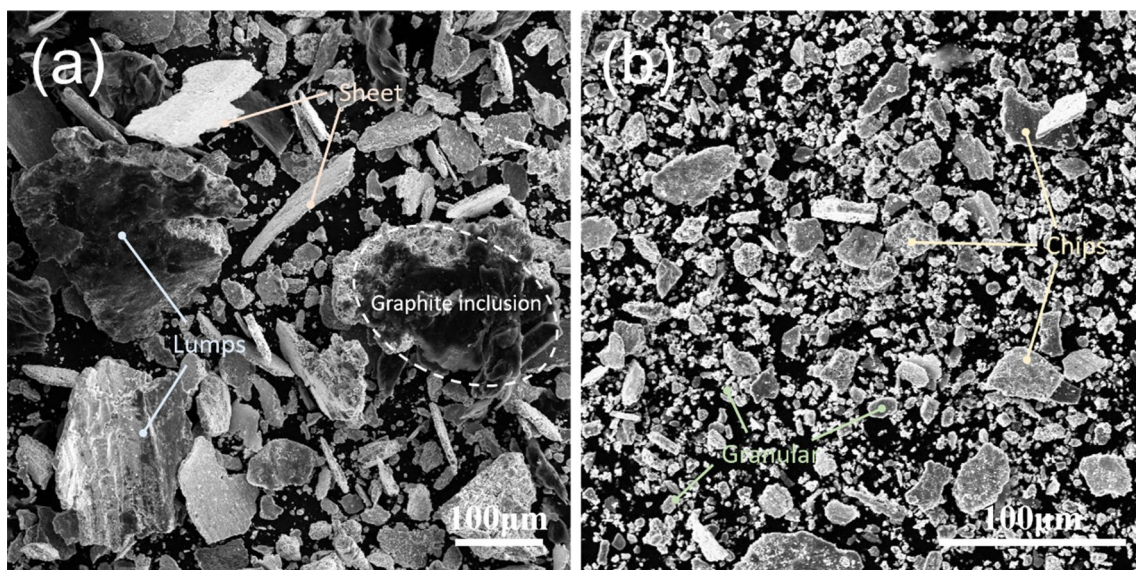


Fig. 11 Typical microstructures of the wear debris. **a** S1; **b** S4

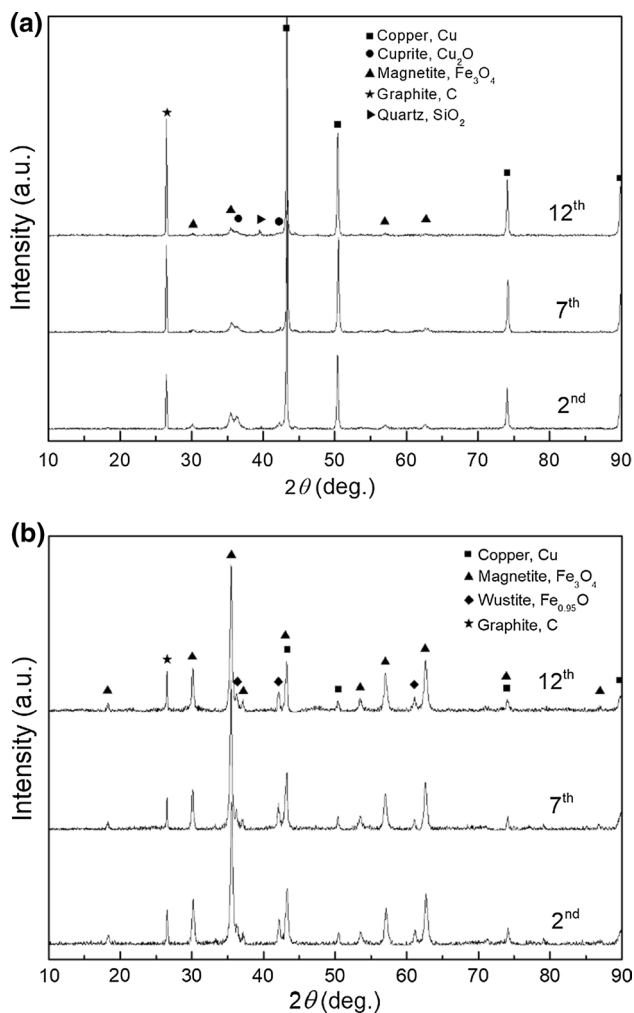


Fig. 12 XRD patterns of the wear debris of **a** S1 and **b** S4 with regard to different braking times

Acknowledgements The financial support from National Natural Science Foundation of China under Contract No. 51572026 is gratefully acknowledged.

References

- Natarajan, N., Vijayarangan, S., Rajendran, I.: Wear behavior of A356/25SiCp aluminum matrix composites sliding against automobile friction material. *Wear* **261**, 812 (2006)
- Zhou, X., Zhu, D., Xie, Q., Luo, F., Zhou, W.: Friction and wear properties of C/C–SiC braking composites. *Ceram. Int.* **38**, 2467 (2012)
- Xiong, X., Chen, J., Yao, P., Li, S., Huang, B.: Friction and wear behaviors and mechanisms of Fe and SiO_2 in Cu-based P/M friction materials. *Wear* **262**, 1182 (2007)
- Chen, B., Bi, Q., Yang, J., Xia, Y., Hao, J.: Tribological properties of solid lubricants (graphite, h-BN) for Cu-based P/M friction composites. *Tribol. Int.* **41**, 1145 (2008)

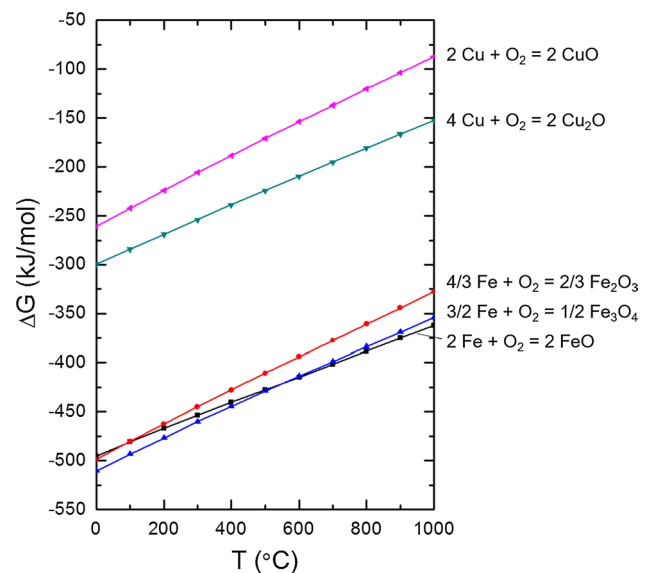


Fig. 13 Simplified Ellingham diagram indicating the relative free energies for various metal oxidation reactions [30]

- Li, G., Yan, Q.: Comparison of friction and wear behavior between C/C, C/C–SiC and metallic composite materials. *Tribol. Lett.* **60**, 15 (2015)
- Li, G., Yan, Q., Xi, J., Qi, G., Yang, X.: The stability of the coefficient of friction and wear behavior of C/C–SiC. *Tribol. Lett.* **58**, 13 (2015)
- Bao, J., Zhu, Z., Yin, Y., Chen, G.: Influence of initial braking velocity and braking frequency on tribological performance of non-asbestos brake shoe. *Ind. Lubr. Tribol.* **61**, 332 (2009)
- Ścieszka, S.F.: Tribological phenomena in steel-composites brake materials friction pairs. *Wear* **64**, 367 (1980)
- Rhee, S.K.: Wear equations for polymers sliding against metal surfaces. *Wear* **16**, 431 (1970)
- Talib, R.J., Muchtar, A., Azhari, C.H.: Microstructural characteristics on the surface and subsurface of semimetallic automotive friction materials during braking process. *J. Mater. Process. Technol.* **140**, 694 (2003)
- Zhu, Z., Bao, J., Yin, Y., Chen, G.: Frictional catastrophe behaviors and mechanisms of brake shoe for mine hoisters during repetitive emergency brakings. *Ind. Lubr. Tribol.* **65**, 245 (2013)
- Verma, P.C., Ciudin, R., Bonfanti, A., Aswath, P., Straffellini, G., Gialanella, S.: Role of the friction layer in the high-temperature pin-on-disc study of a brake material. *Wear* **346–347**, 56 (2016)
- Peng, T., Yan, Q., Li, G., Zhang, X., Wen, Z., Jin, X.: The braking behaviors of Cu-based metallic brake pad for high-speed train under different initial braking speed. *Tribol. Lett.* **65**, 135 (2017). <https://doi.org/10.1007/s11249-017-0914-9>
- Österle, W., Urban, I.: Friction layers and friction films on PMC brake pads. *Wear* **257**, 215 (2004)
- Österle, W., Urban, I.: Third body formation on brake pads and rotors. *Tribol. Int.* **39**, 401 (2006)
- Filip, P., Weiss, Z., Rafaja, D.: On friction layer formation in polymer matrix composite materials for brake applications. *Wear* **252**, 189 (2002)
- Jacko, M.G., Tsang, P.H.S., Rhee, S.K.: Wear debris compaction and friction film formation of polymer composites. *Wear* **133**, 23 (1989)

18. Peng, T., Yan, Q., Li, G., Zhang, X.: The influence of Cu/Fe ratio on the tribological behavior of brake friction materials. *Tribol. Lett.* **66**, 18 (2018). <https://doi.org/10.1007/s11249-017-0961-2>
19. Desplanques, Y., Degallaix, G.: Interactions between third-body flows and localisation phenomena during railway high-energy stop braking. *SAE Int. J. Passeng. Cars Mech. Syst.* **1**, 1267 (2008)
20. Godet, M.: The third-body approach: a mechanical view of wear. *Wear* **100**, 437 (1984)
21. Desplanques, Y., Degallaix, G.: Genesis of the third-body at the pad-disc interface: case study of sintered metal matrix composite lining material. *SAE Int. J. Mater. Manuf.* **2**, 25 (2010)
22. Haddad, H., Guessasma, M., Fortin, J.: A DEM–FEM coupling based approach simulating thermomechanical behaviour of frictional bodies with interface layer. *Int. J. Solids Struct.* **81**, 203 (2016)
23. Österle, W., Dörfel, I., Prietzel, C., Rooch, H., Cristol-Bulthé, A.L., Degallaix, G., Desplanques, Y.: A comprehensive microscopic study of third body formation at the interface between a brake pad and brake disc during the final stage of a pin-on-disc test. *Wear* **267**, 781 (2009)
24. Rigney, D.A., Hirth, J.P.: Plastic deformation and sliding friction of metals. *Wear* **53**, 345 (1979)
25. Österle, W., Kloß, H., Urban, I., Dmitriev, A.I.: Towards a better understanding of brake friction materials. *Wear* **263**, 1189 (2007)
26. Österle, W., Dmitriev, A.I.: Functionality of conventional brake friction materials—perceptions from findings observed at different length scales. *Wear* **271**, 2198 (2011)
27. Archard, J.F., Hirst, W.: The wear of metals under unlubricated conditions. *Proc. R. Soc. Lond. A* **236**, 397 (1956)
28. Stott, F.H.: High-temperature sliding wear of metals. *Tribol. Int.* **35**, 489 (2002)
29. Kato, H., Komai, K.: Tribofilm formation and mild wear by tribosintering of nanometer-sized oxide particles on rubbing steel surfaces. *Wear* **262**, 36 (2007)
30. Blau, P.J.: Elevated-temperature tribology of metallic materials. *Tribol. Int.* **43**, 1203 (2010)
31. Jiang, J., Stott, F.H., Stack, M.M.: The role of triboparticles in dry sliding wear. *Tribol. Int.* **31**, 245 (1998)
32. McNeill, L.S., Edwards, M.: The importance of temperature in assessing iron pipe corrosion in water distribution systems. *Environ. Monit. Assess.* **77**, 229 (2002)
33. Rakhshani, A.E.: Preparation, characteristics and photovoltaic properties of cuprous oxide—a review. *Solid State Electron.* **29**, 7 (1986)
34. Suh, N.P., Sin, H.C.: The genesis of friction. *Wear* **69**, 91 (1981)